3rd URSI AT-AP-RASC, Gran Canaria, 29 May – 3 June 2022

3D Miniaturization Method and its Application to a Wearable Vivaldi Antenna

Mehmet Akif Acar*(1), Ozan Furkan Sezgen(1), Oğuz Kaan Erden(1), and Sema Dumanli(1)
(1) Bogazici University, Electrical and Electronics Engineering, Istanbul, Turkey

Abstract

This work describes an antenna miniaturization method that utilizes meandering in the third dimension. The radiator of the antenna is designed on a corrugated substrate. Semi-cylindrical, triangular, and rectangular corrugations are tried. The method is applied to an Ultra-wideband Vivaldi antenna. The antenna is proposed to be 3D printed on IBT, a flexible and biocompatible resin, for the first time in the literature. By this method, three different miniaturized Vivaldi antennas are designed, and up to 22.1% reduction in the volume is achieved.

1 Introduction

Recently 3D printing technology has been used in industrial and medical applications, which reduces the manufacturing time and cost and facilitates the process of controlling the shape of complex structures and properties of the required substrates [1]. There are multiple categories of 3D printing processes: material extrusion, light polymerization, powder bed fusion, material jetting, etc. For antenna prototyping, Fused Deposition Modelling and Stereolithography (SLA) have been commonly used, which falls under material extrusion and light polymerization, respectively.

Commonly used rigid substrates such as acrylonitrile-butadiene-styrene [2]–[4], polylactic acid [5]–[8], and V04 [9] are not suitable for wearable antennas envisaged for modern health monitoring systems and daily life wireless devices [10]. As a result, the focus moves towards utilizing flexible and elastic substrates. Thus, they can be integrated into clothes and wearable devices to be operated on curvilinear surfaces and dynamically changing motions. FLGR02, IBT, 50A, and 80A resins are flexible materials available in SLA technology. FLGR02 has previously been used in antenna prototyping [11]. However, IBT, 50A and 80A have never been used. Here, using these substrates, we proposed a 3D miniaturization method which is based on [12]. The method is demonstrated through a Vivaldi antenna.

UWB is becoming more popular in implant communications, which crave UWB wearable, flexible repeater antennas. Vivaldi antenna is a frequent choice for applications that require wide bandwidth [13]. There are multiple examples of rigid 3D printed Vivaldi antennas [14], [15] and flexible Vivaldi antennas in the literature [16]–[18]. However, there is no flexible 3D printed Vivaldi antenna in the literature to the best of the authors' knowledge. In this paper, the novelty lies in the application of the 3D miniaturization method on a flexible wearable Vivaldi antenna. In addition, the electrical properties of previously mentioned flexible resins are provided up to 6 GHz for the first time in the literature.

This paper is organized as follows. Section II describes the Vivaldi antenna model, and three different corrugations are presented. The simulation results are demonstrated in Section III. Section IV concludes the paper.

2 Antenna Models

Vivaldi antennas have exponentially tapered slots following Eqn. 1 where A is half of the minimum width of the tapered slot, k is the taper rate, and y(x) is the half-width of the tapered slot. The maximum width of the taper must be less than half of the guided wavelength of the minimum operating frequency [19].

$$y(x) = Ae^{kx} \tag{1}$$

2.1 Model A

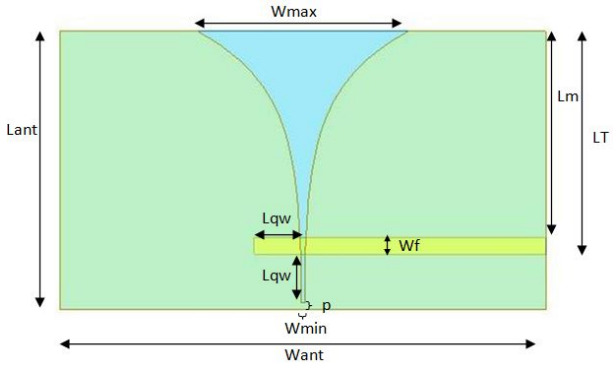

Figure 1. The Vivaldi antenna designed on flat flexible IBT

Figure 1 shows the microstrip fed Vivaldi antenna designed following these guidelines. The design is on flexible IBT resin (Model A). Figure 2 presents the relative permittivity and conductivity values of IBT along with two more flexible resins measured up to 6 GHz. The measurements are

conducted using Speag's DAKS 3.5 dielectric measurement kit at room temperature.

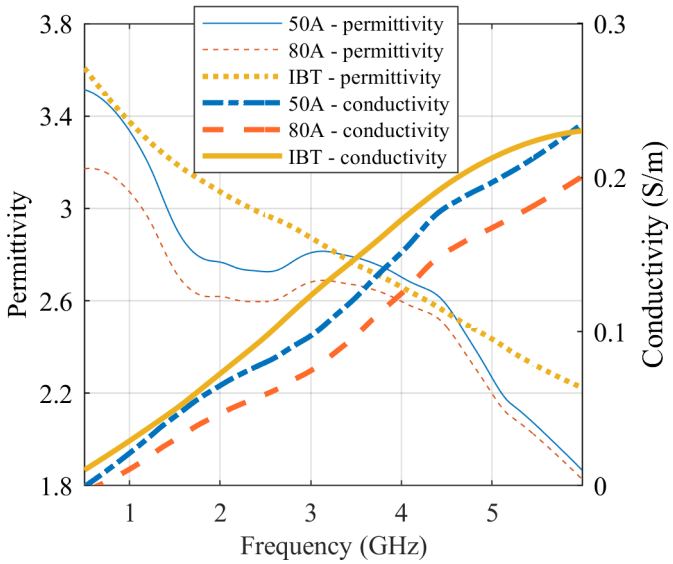

Figure 2. Measured relative permittivity and conductivity values for flexible resins available for SLA printing: 50A, 80A, and IBT vs frequency

The feed line is open-circuited at a distance from the center of the tapered slot, and this distance is adjusted to Lqw=1.5 mm to achieve intended matching. The antenna is optimized to operate on a 2 cm thick muscle block representing the human body using ANSYS HFSS. The first model constitutes the base for the other three miniaturized versions, with different substrate structures. For miniaturization purposes, triangular, cylindrical, and square corrugations are added to the substrate. All the parameters are kept constant in these models regarding the radiator and the feed line. Thus, the antenna's overall length is decreased by wrapping the same radiator onto the new substrate profiles. By doing so, both the volume and the overall size of the antennas are decreased.

The top view and the parameters of the designed Vivaldi antenna on a planar substrate are shown in Figure 1. The minimum width of the tapered slot is chosen as Wmin=0.3 mm, while its maximum width is limited by half of the guided wavelength at the minimum operating frequency, $\lambda_g/2$=15.3 mm. λ_g is calculated by using Eqn. 2, where c is the speed of light, f_{min} is the minimum operating frequency, 3.1GHz, and ε_{eff} is the effective permittivity of the medium. The effective permittivity is chosen as 10 in the calculation by considering that the antenna is working on an IBT substrate located on the muscle block.

$$\lambda_g = \frac{c}{\sqrt{\varepsilon_{eff}} f_{min}}. \quad (2)$$

*L*T is chosen as 16 mm. In order to achieve a width less than $\lambda_g/2$ = 15.3 mm with a 16 mm length, the taper rate, k, is chosen as 0.245. The maximum width, Wmax, is then calculated as 15.12 mm. Substrate thickness, h, is 0.8 mm, the width of the feed, Wf, is 1.2 mm, and the overall width of the antenna, Want, is 34.9 mm. Lm, 14.8 mm, is the dimension that will be miniaturized, and it is chosen as the difference between LT and Wf not to affect the feed mechanism. Lastly, the antenna's overall length, Lant, is 18 mm. The non-slotted part of the radiator has a length of p=0.5 mm. The volume of Model A is 502.56 mm^3.

2.2 Model B

The second model is designed to have a substrate such that 10 triangular corrugations are added on the planar substrate used in Model A. Triangles are isosceles with equal angles of 45^o. The total length of the edges, each having a length of 0.74 mm, is equal to the initial value of Lm, 14.8 mm. This choice results in a decrease by cos(45^o), approximately 29.8%, in Lm. Compared to Model A, the length of Model B is decreased by 24.1%, from 18mm to 13.66 mm. Finally, the volume of the antenna is 477.08 mm^3, corresponding to a decrease of 5.07%. Model B is shown in Figure 3.

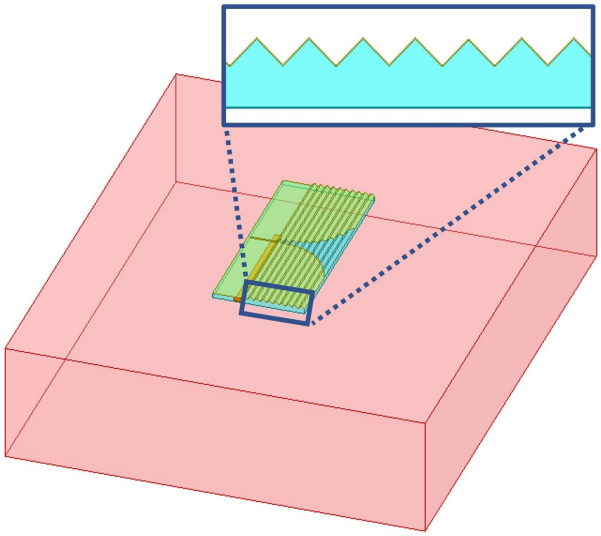

Figure 3. 3D view of Model B

2.3 Model C

By adding 10 semi-cylindrical corrugations onto the planar substrate, a 29.8% decrease in length is achieved. Model C has a Lant of 12.62 mm. The radius of the semi-cylinders, Rc, is adjusted to be 0.47 mm such that their total perimeter is equal to the initial length of 14.8 mm. This choice of radius results in a decrease of approximately 36% (2/π) in Lm. Moreover, the volume is decreased to 473.45 mm^3, which is 5.79% smaller than the initial volume. The isometric view of Model C is shown in Figure 4.

2.4 Model D

Model D has 5 square corrugations with equal side lengths of 0.74 mm, for both square prisms and their spaces. By doing so, Lm is halved. Model D's isometric view is shown in

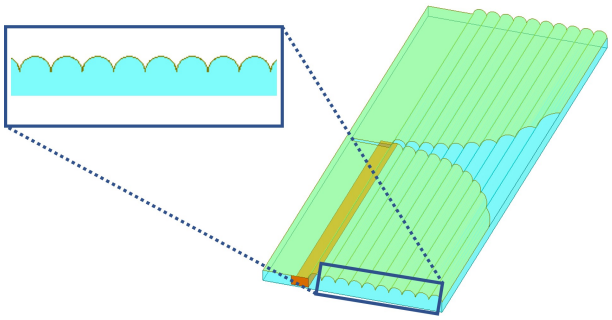

Figure 4. Isometric View of Model C and the corrugation profile.

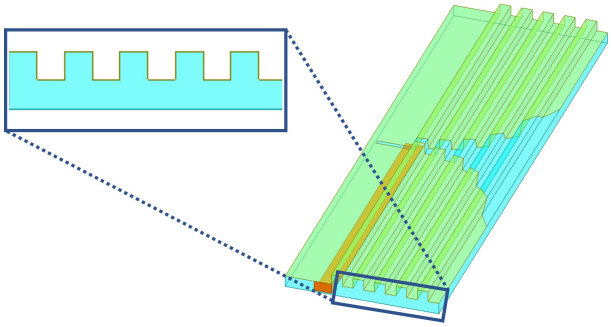

Figure 5. Isometric View of Model D and the corrugation profile.

Figure 5. The length is 10.6 mm, and the volume is 391.51 mm^3, which corresponds to a decrease of 41.1% and 22.1%, respectively.

3 Simulations and Results

When the miniaturized models are compared to Model A, 5.07%, 5.79%, and 22.1% decrease in the volume and 24.1%, 29.8%, and 41.1% decrease in the length is achieved for Model B, Model C, and Model D, respectively. The resulting reflection coefficients are plotted in Figure 6. All four models cover the lower UWB frequency range. Figure 7a shows the simulated 2D radiation patterns at $\phi = 0^\circ$ and $\phi = 90^\circ$ at 3.44, 3.27, 3.2, and 3.18 GHz for each model, respectively. Note that, these frequency points correspond to the first resonances of the antennas. Similarly, Figure 7b shows the 2D radiation patterns at 5.74, 5.72, 5.66, 5.78 GHz. The maximum gain values for each model are compared in Table 1. As can be seen from the table, miniaturization decreases the maximum gain values for the first resonances while it does not impact the gain for the second resonances. When it comes to the maximum radiation direction, no more than 6° change is observed in θ and ϕ for the lower resonances. However, the maximum radiation direction changes towards the muscle block for the higher frequency resonance.

4 Conclusion

A 3D miniaturization method that utilizes meandering in the third dimension is described for an UWB Vivaldi antenna. Miniaturization is attained by adding semi-cylindrical, triangular and square prisms over the base substrate. 5.07%, 5.79%, 22.1% volume decrease relative to initial model is obtained, for Model B, Model C, and Model D, respectively. In conclusion, lower UWB characteristics of the antennas are maintained while a reduction in volume is acquired. However, the maximum gain values of the miniaturized models decrease when the miniaturization ratio is increased.

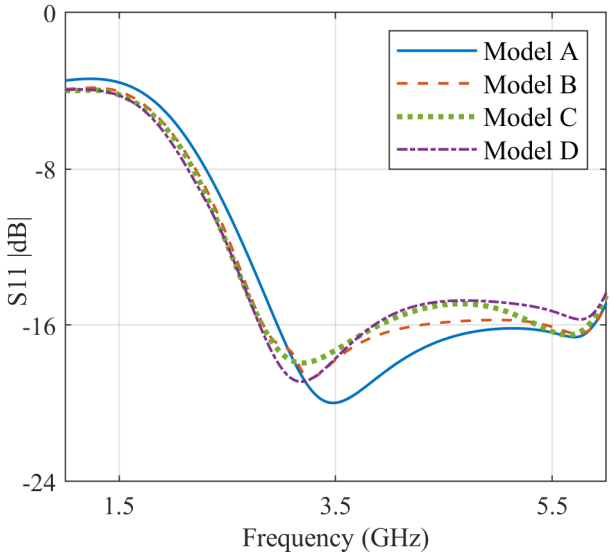

Figure 6. $|S11|$ vs. frequency (GHz) plots for each model.

Table 1. The maximum gain directions in dBi

	1^{st} *Resonance*			2^{nd} *Resonance*		
	Gain	θ°	ϕ°	Gain	θ°	ϕ°
Model A	-16.6	38	-28	-13.4	8	30
Model B	-16.6	40	-18	-11.8	14	-26
Model C	-17.1	40	-14	-11.5	14	-32
Model D	-17.9	42	-10	-11.6	16	-48

5 Acknowledgements

This work was supported in part by Bogazici University Scientific Research Fund (BAP) under project number BAP 18202 and the Scientific and Technical Research Council of Turkey (TUBITAK) under Grant 120C131.

References

[1] M. Rizwan, M. W. A. Khan, L. Sydanheimo, J. Virkki, and L. Ukkonen, "Flexible and Stretchable Brush-Painted Wearable Antenna on a Three-Dimensional (3-D) Printed Substrate," IEEE Ant. Wirel. Propag. Lett., vol. 16, pp. 3108–3112, 2017.

[2] M. Mirzaee and S. Noghanian, "Additive manufacturing of a compact 3D dipole antenna using ABS thermoplastic and high temperature carbon paste," 2016

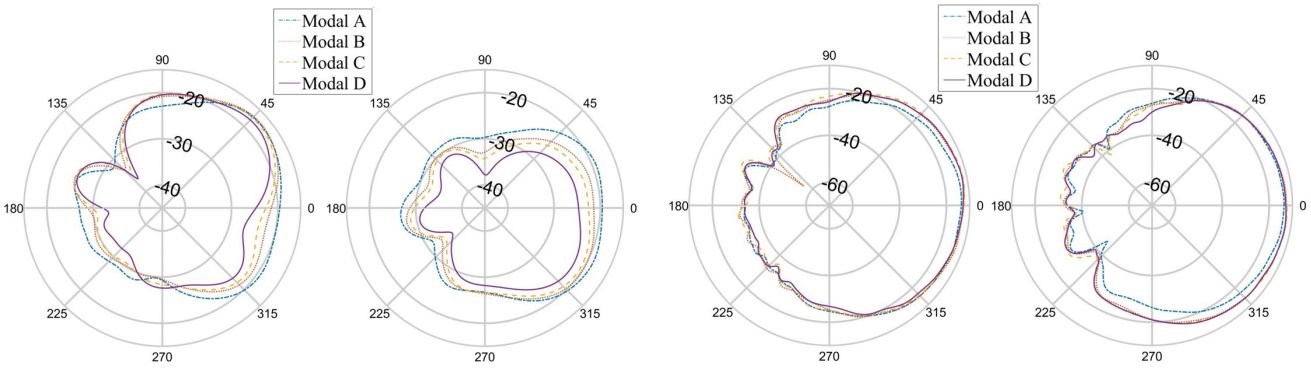

(a) First resonance frequency

(b) Second resonance frequency

Figure 7. 2D Radiation Patterns of All Models at $\phi = 0°$(left) and $\phi = 90°$(right).

IEEE Antennas Propag. Soc. Int. Symp. APSURSI 2016 - Proc., vol. 1, pp. 475–476, 2016.

[3] L. Wu, H. Chu, D. Cao, S. Peng, and Y. Guo, "3-D Printed Antenna Subsystem with Dual-Polarization and its Test in System Level for Radiometer Applications," IEEE Access, vol. 8, pp. 127856–65, 2020.

[4] H. Islam, S. Das, T. Bose, and S. Dhar, "High efficient dual band stacked antennas integrated into rescue helmets for indoor communication," Int. J. Microw. Wirel. Technol., 2020.

[5] C. Prakash, P. Senthil, and T. Sathies, "Fused deposition modeling fabricated PLA dielectric substrate for microstrip patch antenna," Mater. Today Proc., vol. 39, pp. 533–537, 2020.

[6] M. Czelen, M. Rzymowski, K. Nyka, and L. Kulas, "Miniaturization of ESPAR Antenna Using Low-Cost 3D Printing Process," 14th Eur. Conf. Antennas Propagation, EuCAP 2020, pp. 3–6, 2020.

[7] N. Alias, S. M. Shaharum, and M. S. A. Karim, "Design of a 3D Printed UWB Antenna for a Low-Cost Wireless Heart and Respiration Rate Monitoring," IOP Conf. Ser. Mater. Sci. Eng., vol. 917, no. 1, 2020.

[8] P. Parthiban, B. C. Seet, and X. J. Li, "3D-printed circularly polarized concave patch with enhanced bandwidth and radiation pattern," Microw. Opt. Technol. Lett., vol. 63, no. 2, pp. 572–580, 2021.

[9] V. Marrocco et al., "Rapid Prototyping of Bio-Inspired Dielectric Resonator Antennas for Sub-6 GHz Applications," Micromachines, vol. 12, no. 9, p. 1046,2021.

[10] S. G. Kirtania et al., "Flexible antennas: A review," Micromachines, vol. 11, no. 9, 2020.

[11] Y. Cui, S. A. Nauroze, R. Bahr, and E. M. Tentzeris, "3D printed one-shot deployable flexible 'kirigami' dielectric reflectarray antenna for mm-Wave applications," IEEE MTT-S Int. Microw. Symp. Dig., vol. 2020-Augus, pp. 1164–1167, 2020.

[12] J. O'Brien et al., "Miniaturization of microwave components and antennas using 3D manufacturing," 2015 9th European Conference on Antennas and Propagation (EuCAP), 2015, pp. 1-4.

[13] A. M. de Oliveira et al., "A Fern Antipodal Vivaldi Antenna for Near-Field Microwave Imaging Medical Applications," in IEEE Transactions on Ant. and Prop., vol. 69, no. 12, pp. 8816-8829, Dec. 2021.

[14] M. I. M. Ghazali, K. Y. Park, J. A. Byford, J. Papapolymerou and P. Chahal, "3D printed metalized-polymer UWB high-gain Vivaldi antennas," 2016 IEEE MTT-S International Microwave Symposium (IMS), 2016, pp. 1-4.

[15] L. Zhou, M. Tang and J. Mao, "3-D Printed Vivaldi Antenna Fed by SIW Slot for Millimeter-Wave Applications," 2021 International Conference on Microwave and Millimeter Wave Technology (ICMMT), 2021, pp. 1-3.

[16] Al-Janabi, Mustafa Kayhan, Sema. (2020). Flexible Vivaldi Antenna Based on a Fractal Design for RF-Energy Harvesting. Progress In Electromagnetics Research M. 97. 177-188.

[17] Saeidi, Tale et al. (2020). Metamatrial-based Antipodal Vivaldi Wearable UWB Antenna for IoT and 5G Applications.

[18] P. Nijhawan, A. Kumar and Y. Dwivedi, "A flexible corrugated vivaldi antenna for radar and see-through wall applications," 2018 3rd International Conference on Microwave and Photonics (ICMAP), 2018, pp. 1-2.

[19] C. A. Balanis, Antenna theory: Analysis and Design. John Wiley & Sons, 2016.